\$ STORY IN THE SERVICE RELATIONS AND ADMINISTRATION OF THE SERVICE RELATION OF THE SERVICE RESPONDED OF THE SERVICE RESPONDED

Contents lists available at ScienceDirect

Journal of Colloid And Interface Science

journal homepage: www.elsevier.com/locate/jcis



Regular Article

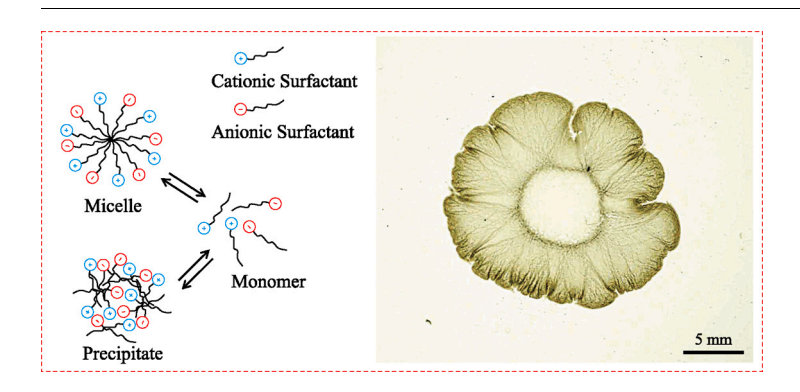
Marangoni flows triggered by cationic-anionic surfactant complexation

Ali Nikkhah, Sangwoo Shin 3

Department of Mechanical and Aerospace Engineering, University at Buffalo, The State University of New York, Buffalo, NY 14260, USA



GRAPHICAL ABSTRACT



ARTICLE INFO

Keywords: Surfactants Marangoni flows Complexation Surface tension Reaction kinetics

ABSTRACT

Hypothesis: The gradients in surfactant distribution at a fluid-fluid interface can induce fluid flow known as the Marangoni flow. Fluid interfaces found in biological and environmental systems are seldom clean, where mixtures of various surfactants are present. The presence of multi-component surfactant mixtures introduces the possibility of interactions among constituents, which may impact Marangoni flows and alter flow dynamics.

Experiments: We employed flow visualization, surface tension and reaction kinetic measurements, and numerical simulations to quantitatively investigate the Marangoni flows induced by the reacting surfactant mixtures. Different binary surfactant mixtures were utilized for comparative analysis.

Findings: The impact of surfactant interactions on Marangoni flows is confirmed through the observation of diverse complex flow patterns that result from the combination of oppositely charged surfactants in varying composition ratios and concentrations. Unique flow patterns originate from the composition-dependent interfacial phenomena upon mixing surfactants. Our findings provide vital insights that could be used to guide the development of effective oil remediation or the spreading of waterborne pathogens in contaminated regions.

1. Introduction

Surface active compounds, also known as surfactants, are a class of molecules that may alter the surface tension at a fluid-fluid interface.

The occurrence of non-uniform surfactant distribution throughout the fluid interface causes gradients in the surface tension, resulting in the motion of fluid from regions of low to regions of high surface tension. This phenomenon, commonly referred to as Marangoni flow, plays a cru-

E-mail address: sangwoos@buffalo.edu (S. Shin).

https://doi.org/10.1016/j.jcis.2024.07.014

^{*} Corresponding author.

cial role in many natural phenomena, like enabling the locomotion of arthropods such as *Microvelia* and *Stenus* on the surface of water by releasing chemicals to create Marangoni propulsion [1]. It is also utilized in numerous industrial applications, such as coatings [2–4], enhanced oil recovery [5,6], drug delivery [7], desalination [8], and biomimicry robots [9].

Due to its importance, extensive efforts have been dedicated in recent years to expand the fundamental understanding of Marangoni flows in more complex surfactant systems, both experimentally [10-14] and numerically [12,15,16]. For instance, Sauleda et al. examined the effect of Marangoni spreading in the presence of insoluble pre-deposited surfactants [10]. They found that surfactant modifies the gradient of surface tension and influences the Marangoni spreading by extending the gradient region of the pre-deposited monolayer. Kim et al. investigated the impact of surfactant-contaminated liquid on Marangoni spreading when an isopropyl alcohol droplet is added to the liquid bath [11]. They reported that Marangoni-driven circulating flow with non-uniform surfactant distribution causes a difference in surfactant concentrations between the adsorbed layer and bulk liquid below the critical micelle concentration (CMC), leading to two opposite Marangoni effects and a rapid decay in flow speed along the radial direction compared to a pure system without surfactants. Mandre [15] examined analytically and numerically the spreading of surfactant from a single point source in an axisymmetric system. Sauleda et al. [16] conducted a numerical study on surfactant spreading behaviors for insoluble and soluble surfactants.

The vast majority of prior studies on Marangoni flows have mainly been concerned with a single type of surfactant and have not considered the impact of irreversible reactions and interactions between multiple constituents. It is only recently that people have started to look into how the interacting surfactants affect the Marangoni flows. For instance, Hsieh et al. reported the effect of binary surfactant mixtures on Marangoni spreading, where the binary surfactants induce synergetic effects on lowering surface tension, and the degree of surface tension reduction was shown to be sensitive to interaction strength [12]. Nguindjel and Korevaar studied the self-sustained Marangoni flows driven by chemical reactions, where a photoreactive chemical process that consumes surfactant at the interface was utilized to drive a long-lasting Marangoni flow [13].

In this study, we examine the effects of the interactions between cationic and anionic surfactants on Marangoni flows, where a strong ionic interaction between oppositely charged surfactants leads to the formation of irreversible complexation [17]. The surfactant complexation at relatively high surfactant concentrations can significantly alter the flow patterns, creating various non-monotonic flows. We rationalize our findings through high-speed flow visualization, surface tension and reaction kinetic measurements, and numerical simulations.

2. Experimental

2.1. Materials

Cetylpyridinium chloride (CPC), cetrimonium bromide (CTAB), sodium dodecylsulfate (SDS), and Triton X-100 were purchased from Sigma Aldrich. These surfactants were dissolved in deionized water to prepare surfactant solutions with concentrations ranging from 0.01 mM to 100 mM. Silver-coated hollow ceramic particles (diameter = $150\,\mu m$) for flow tracers were purchased from Cospheric.

2.2. Flow visualization

To capture the rapid movement of tracer particles, we utilized a highspeed camera (Phantom V9.1), adjusting the frame rate accordingly for each experiment. The particle Stokes number was estimated to be much less than unity, indicating excellent flow tracing fidelity. More details regarding the estimation of the particles' Stokes number can be found in Supporting Materials. After recording, we analyzed the videos using ImageJ and MATLAB (PIVlab) to measure the flow field. A 10 μL droplet was gently transferred to the center of a Petri dish (diameter =14 cm, depth =1 cm) filled with aqueous surfactant solution and tracer particles using a micropipette.

2.3. Thermal imaging

We used an infrared thermal camera (E60, FLIR) to detect heat generation during the mixing of CPC and SDS (Fig. S3). To minimize disturbances and ensure accurate readings, we placed Petri dish samples on a black blanket and adjusted the camera distance to match the focal point.

2.4. Surface tension measurement

The pendant drop method was used to measure the surface tension of CPC, SDS, and their mixture solutions using a camera (D3400, Nikon), syringe, blunt-tip needle, and an LED backlight (Phlox). An in-house MATLAB code was used to detect the droplet curvature and numerically solve the Young-Laplace equation to obtain the surface tension [18].

2.5. Reaction kinetic measurement

We employed a spectrophotometric approach to acquire kinetic constants for various concentrations of surfactant mixtures [19,20]. The cuvettes were filled with a volume of 2 ml of surfactant solution, followed by the careful injection of the counterion surfactant using a syringe. The kinetic order and coefficients were determined by measuring the light transmittance (at 600 nm) over time using a dynamic light scattering instrument (Litesizer 500, Anton Paar).

3. Results and discussion

3.1. Non-monotonic Marangoni flows induced by surfactant mixing

By introducing a minute droplet (volume = $10\,\mu\text{L}$) of cationic surfactants (cetylpyridinium chloride, CPC) into a bath of anionic surfactants (sodium dodecylsulfate, SDS), and vice versa, we observe various flow patterns resulting from the reactive transport of cationic-anionic surfactant mixtures induced by surfactant-surfactant complexation. The high-speed imaging of the flow patterns visualized by the tracer particles (silver-coated hollow ceramic particles, diameter $d_p = 150\,\mu\text{m}$) is shown in Fig. 1a-d, with their accompanying kymographs presented in Fig. 1e-h.

In scenarios involving low SDS concentration in the bath (≤ 1 mM) with a wide range of CPC concentrations in the droplet (0.1-100 mM), an initial outward flow followed by a relatively fast inward flow is observed (outward-inward flow; OI) (Figs. 1a,e, Movie S1). The same OI behavior is observed for bath with low CPC concentrations (< 1 mM). For systems characterized by moderate-to-high CPC-SDS concentrations (SDS concentration of 2.5–100 mM and CPC concentration of 0.1–25 mM) exhibit an oscillatory flow (Figs. 1b,f, Movie S2). This flow was solely observed in the CPC bath with a similar flow behavior to OI (both experience outward flow then inward flow), albeit with the distinction that the outward flow undergoes an oscillatory flow at a frequency of about 10 Hz. We note that this frequency is sensitive to the concentration and ratio of surfactants.

When highly concentrated surfactant droplets (> 25 mM) are deposited onto a bath of highly concentrated solution of oppositely charged surfactants, they induce an initial outward flow, followed by a rapid inward flow, and eventually transition into a gradual outward flow, showcasing an outward-inward-outward (OIO) flow pattern accompanied by visible surfactant precipitation (Figs. 1c,g, Movie S3). The presence of precipitation indicates a strong ionic reaction between the constituents at high surfactant concentrations [21].

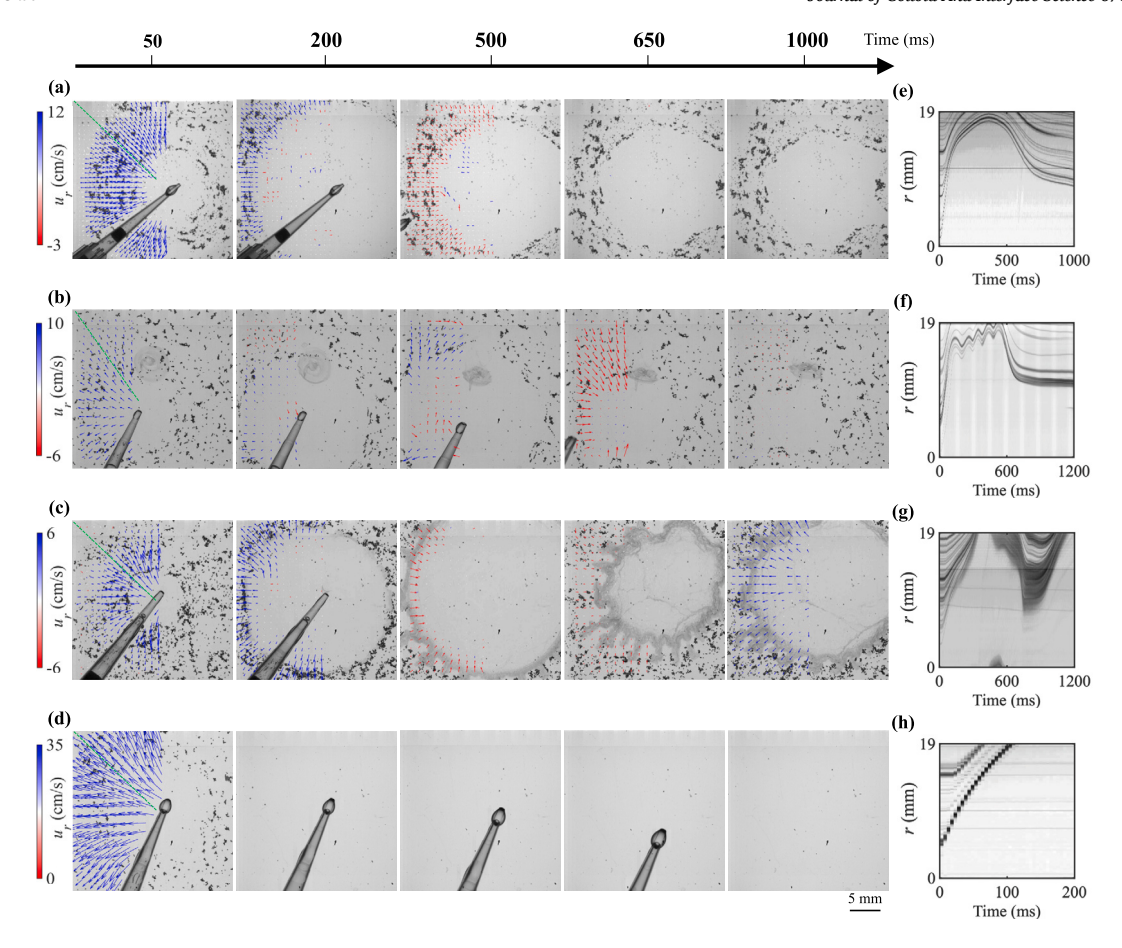


Fig. 1. Various Marangoni flow patterns observed upon introduction of a small drop of ionic surfactants to a bath of oppositely charged surfactants. (a-d) Image sequences and (e-h) corresponding kymographs taken along the radial direction (green lines in (a-d). The coordinate origin is located at the center of the droplet). Observed flow patterns are mainly categorized into four unique behaviors. These behaviors are (a,e) outward-inward (droplet = CPC, 10 mM, bath = SDS, 1 mM), (b,f) oscillation (droplet = SDS, 100 mM, bath = CPC, 1 mM), (c,g) outward-inward-outward (droplet = SDS, 100 mM, bath = CPC, 50 mM), and (d,h) only outward (droplet = CPC, 100 mM, bath = SDS, 1 mM). These observations are also available in Movies S1-S4 (Supporting Materials). The velocity vectors obtained from PIV measurements are partially overlaid on the images, where the blue arrows indicate radially outward flow and the red arrows show inward flow with the color variation representing the radial velocity component u_r . (For interpretation of the colors in the figure(s), the reader is referred to the web version of this article.)

Lastly, when a droplet of moderate-to-high concentration of CPC (> 20 mM) is introduced into a bath of extremely low SDS concentration (< 1 mM) or pure water, only a rapid outward flow is observed (Figs. 1d,h, Movie S4), displaying a typical unidirectional Marangoni flow. The same behavior can also be observed for very low concentrations of CPC in the bath.

The non-monotonic flows (OI, OIO, and oscillation) observed in Figs. 1a-c exhibit inward flows, which demonstrate the potential role of surfactant complexation present at elevated concentrations in the emergence of complex Marangoni patterns. The observed flow patterns can be attained over various ranges of surfactant concentrations and mixing ratios for both SDS and CPC baths, as shown in the phase diagrams in Fig. 2. The phase diagrams indicate that different surfactant types present in both the bath and the droplet have a substantial effect on the flow characteristics. For instance, the deposition of a droplet with a concentration of 50 mM SDS onto a bath containing 50 mM CPC results in an OIO flow pattern. However, the reverse scenario, where a droplet with a concentration of 50 mM CPC is deposited into a bath of 50 mM SDS, does not exhibit the same behavior. As shown in Fig. 2, "no flow" behavior is observed over a broader range of bath concentrations when filled with CPC compared to SDS. This is due to the CPC generally causing lower surface tension compared to SDS across a broader range of concentrations [22]. Consequently, a higher concentration of SDS is required within the droplet to establish a surface tension gradient that generates an initial outward flow.

3.2. Surface tension and reaction kinetics of SDS/CPC mixtures

The phase diagrams in Fig. 2 show that the flow behaviors are not only dependent on the concentration but also the composition ratio. For instance, by maintaining a constant droplet concentration and altering the bath concentration or vice versa, distinct flow patterns can be attained. This indicates that in some cases, despite the surfactant concentration being above the CMC, where the surface tension is nearly independent of the surfactant concentrations, variations in the flow patterns can still be accomplished. These observations suggest that the surfactant mixture involves reactive interactions that affect the surface tension. Moreover, as illustrated in Fig. 1, the observed spatiotemporal shifts in the flow direction during OIO, OI, or oscillation imply the occurrence of dynamic, localized changes in the concentrations of SDS and CPC during the progression of the interaction between SDS and CPC, and thus the surface tension.

In this regard, we performed surface tension measurements using the pendant drop method for varied concentrations and ratios of SDS/CPC, where the measurement results are presented in Fig. 3 [18]. As expected, the surface tension generally goes down with increasing surfactant amount. The surface tension does, however, exhibit multiple local maxima at around equimolar mixture ratio at which precipitation can also be seen. This behavior is a direct indication that the surfactant reactions impact the surface tension, where the production of precipitate results in a decrease in the concentration of SDS and CPC monomers,

 Table 1

 Kinetic coefficients at different surfactant concentrations.

Kinetic type	Very low concentration $(c \le 1 \text{ mM})$		Low concentration $(1 < c \le 10 \text{ mM})$		Intermediate concentration (10 < $c \le 25$ mM)		High concentration $(c > 25 \text{ mM})$	
	v_m	k	v_m	k	v_m	k	v_m	k
Slow ^a	0.775	0.794	1.21	1.47	2.77	11.1	3.80	9.23
Fast ^b	1.10	2.58	31.0	5.07	125	75.0	419	6.59
Combined ^c	-	-	5.55	1.49	5.58	21.3	6.89	20.5

- ^a Reaction rate changes slowly (rate taken from the slope of the reaction curve at the lower asymptote).
- ^b Reaction rate changes abruptly (upper asymptote of the reaction curve).
- ^c All data points are taken into account.

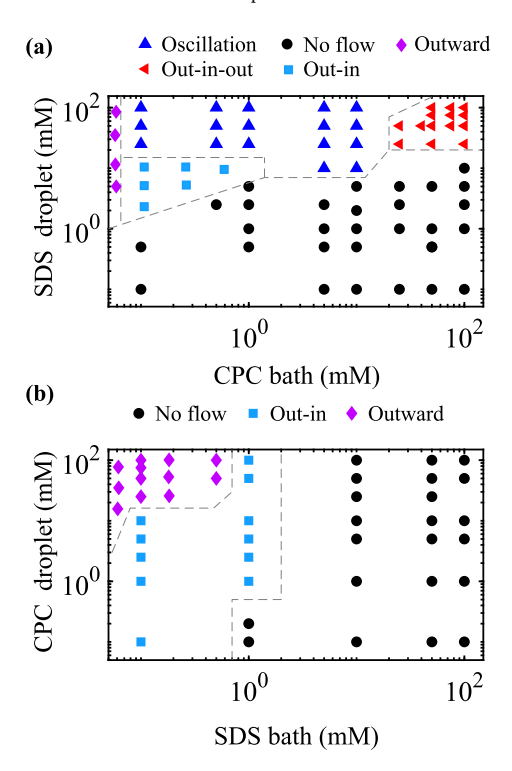


Fig. 2. Phase diagrams revealing various modes of Marangoni flows triggered by surfactant mixing at varying concentrations. (a) CPC bath and SDS droplet. (b) SDS bath and CPC droplet.

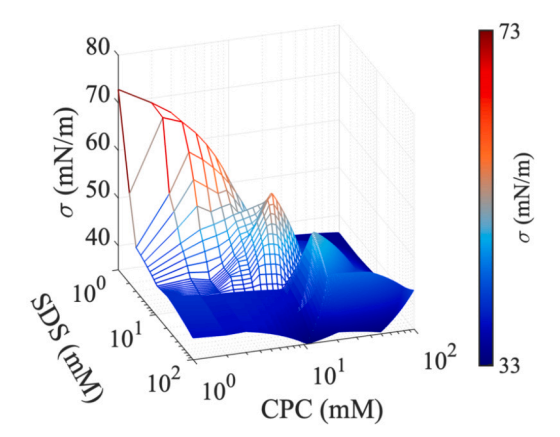


Fig. 3. Surface tension measurements of water-air interface in the presence of SDS and CPC mixture at varying concentrations and mixture ratios.

thereby leading to elevated surface tension [23,24]. This observation contrasts with the synergistic reduction in the surface tension observed in non-reacting binary surfactant mixtures without the formation of precipitation, as reported in the recent study by Hsieh et al. [12].

This interaction has a direct effect on the surface tension and, as a result, plays a crucial role in modifying the direction and the magnitude of the Marangoni stress at the interface. To quantify the interaction between the surfactants, we measured the reaction kinetics using spectrophotometry. Assuming that our system follows the Michaelis-Menten kinetics due to the asymmetry in the amount of surfactants between the bath and the droplet [19,20,25], the reaction rate reads

$$R_c = \frac{v_m c}{k + c},\tag{1}$$

where c is the surfactant concentration of the droplet, v_m is the maximum reaction rate, and k is the Michaelis coefficient. The measured coefficients are tabulated in Table 1 for different surfactant concentrations. Our kinetic measurements show that the interaction between CPC and SDS occurs at two distinct rates (fast and slow). When a droplet of surfactant solution is added to the bath of counterion surfactants, the reaction proceeds at a rapid rate at high concentrations and then gradually slows down, as indicated by the large difference in the reaction rate v_m . On the other hand, this distinct rate change cannot be seen at very low surfactant concentrations as v_m are measured to be relatively similar (e.g., 0.78 for slow and 1.1 for fast kinetics). With increasing surfactant concentrations, v_m rises from 0.78 to 3.8 for slow kinetics and 1.1 to 419 for fast kinetics, indicating stronger ionic interactions at higher concentrations. The rapid, strong surfactant reactions at high concentrations alter the local surfactant concentration gradients, leading to non-monotonic Marangoni patterns such as OIO, OI, or oscillatory flows.

3.3. Reactive transport of surfactant mixtures

To gain a detailed picture of reactive surfactant transport, we conducted numerical simulations of surfactant transport that incorporate the measured reaction kinetic and surface tension data as input parameters. We solve Navier-Stokes and advection-diffusion-reaction equations to model the observed phenomena, which builds on the previous works by Mandre [15] and Hsieh et al. [12]. More details regarding the numerical simulations are provided in the Supporting Materials. We compare the flow velocity at the interface obtained by using particle image velocimetry (PIV) and the numerical simulations at three distinct time points for OIO and OI flows, as shown in Fig. 4. Without the use of any free parameters, we obtain a reasonable agreement in terms of predicting the non-monotonic flow reversals and the velocity magnitude between the data obtained from simulations and the measurements acquired using PIV. The observed flow behaviors are essentially contingent upon the interaction of the constituents, leading to diverse flow behavior at different concentrations and mixing ratios.

The surfactant transport and the resulting surface tension distribution for OIO and OI flows are shown in Fig. 5. For the OIO case (Figs. 5a,b; Movie S5,6), upon the introduction of a 50 mM SDS droplet onto a 50 mM CPC bath, a surface tension gradient is established near the central region ($r \rightarrow 0$), initiating the outward flow (t = 50 ms). Soon after (500 ms), the rapid interaction between SDS and CPC at high concentration triggers inward Marangoni flow. This interaction, characterized by a relatively large reaction rate ($v_m = 419$), represents

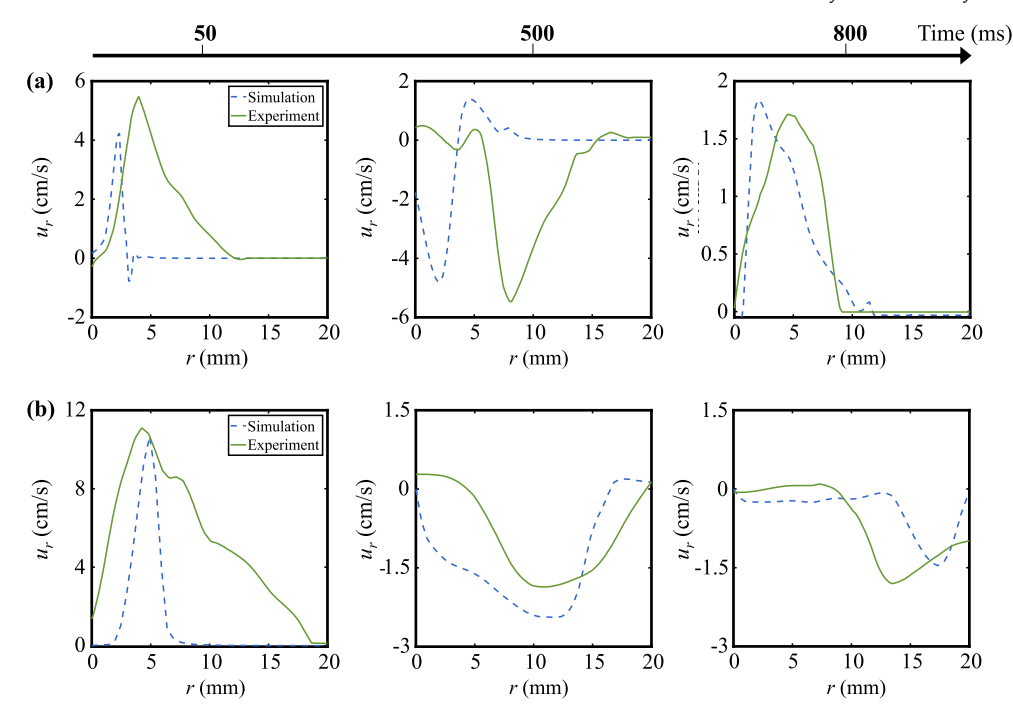


Fig. 4. Comparison of PIV measurements and numerical simulations for the radial flow velocity u_r , for two different flow modes; (a) outward-inward-outward flow (droplet = SDS, 50 mM; bath = CPC, 50 mM) and (b) outward-inward flow (droplet = CPC, 10 mM; bath = SDS, 2 mM).

strong irreversible interactions between the surfactants at high concentrations, which leads to rapid reduction in the SDS concentration. This will, in turn, cause an increase in the surface tension near the central region, leading to inward flow. Then, the reaction gradually slows down ($v_m = 3.8$) with reduced SDS at the interface. Subsequently, this inward flow brings unreacted SDS and CPC from the periphery to the center, which again results in a slight decrease in the surface tension near the center. Such a slight change in the surface tension creates a weak outward flow (800 ms). We note that during the inward flow, weak outward flow concurrently exists at the outer region, as shown in both the PIV measurement and the numerical simulations (black arrows in Fig. 5b at 500 ms). This is attributed to the localized, non-monotonic surface tension gradients established by the concentration-dependent reaction rates.

A comparable transport pattern can also be discerned in the case of OI, despite the absence of a secondary outward flow (Figs. 5c,d; Movie S7,8). When a droplet of 10 mM CPC is introduced to a bath containing 2 mM SDS, the sharp reduction in the surface tension near the center results in a rapid outward flow, which facilitates the transport of unreacted CPC away from the center. As the chemical reaction proceeds and the concentration of CPC decreases in the central region, there is a steady increase in the surface tension, leading to the flow returning towards the center, as seen by the flow field in Fig. 5d at 500 ms. In the long run, the inward flow gradually weakens, which contrasts with the observations shown in Figs. 5a,b where the inward flow is followed by a rather weak outward flow due to the remaining unreacted surfactant species.

The discrepancy between the two flow modes is mainly attributed to the variation in the reaction rate. The kinetic data provided in Table 1 demonstrates a large disparity in v_m between the slow and fast reaction kinetics for both high- and low-concentration scenarios. At early times (<500 ms), the significant reduction in maximum droplet concentration from 50 to 13 mM in the OIO instance, and from 10 mM to 0.9 mM in the OI case, is attributed to initially fast reaction kinetics. At later times (>500 ms), in the OI scenario, the kinetic state remains fast, leading to a nearly complete depletion of surfactant (maximum concentration: 0.9 mM \rightarrow 0.12 mM), whereas in the OIO case reaction slows down so that the reduction in the surfactant concentration is weaker (maximum

concentration: 13 mM \rightarrow 10 mM). Variations in the reaction rate and the distinct surface tension of SDS/CPC mixtures at elevated concentrations lead to the difference between these two cases.

The reactive origin of the OI and OIO flows suggests that Damköhler number may be used to properly characterize the flow modes. While it is difficult to define a single Damköhler number in our system as the flow and the reactions are rapidly changing in time and space, using the simulation data we may define an instantaneous, spatially averaged Damköhler number as

$$\overline{\mathrm{Da}(t)} = \left\langle \frac{R_c(r,t)\ell_\parallel}{u_r(r,t)c(r,t)} \right\rangle,\tag{2}$$

where ℓ_{\parallel} is the characteristic length scale of the flow in the horizontal direction and $\langle \cdot \rangle$ is the spatial average in the horizontal direction over ℓ_{\parallel} along the air-water interface. In Fig. 6, we plot \overline{Da} over the course of simulations (up to 3 seconds), for which we identify distinct ranges of \overline{Da} for different flow modes. As shown, the \overline{Da} is significantly larger for OIO, OI, suggesting that the flow patterns are predominantly influenced by the surfactant reaction. On the other hand, for a low surfactant concentration or in pure water, $\overline{Da} \ll 1$, indicating that reactive transport is negligible. The ranges in which \overline{Da} less than unity in OIO and OI flows correspond to the second outward flow in OIO or the late stages of the inward flow of OI, both of which exhibit weakened reactions.

3.4. Oscillatory flows

The underlying mechanisms that drive OI and OIO Marangoni flows have been fully elucidated through experimental measurements and numerical modeling. Based on the similarities in how the flow behaves, we believe that the Damköhler number for the oscillatory flow should also lie within a similar range to what has been observed in the OIO and OI scenarios. Nevertheless, the current numerical simulations were not able to predict the occurrence of oscillatory flow patterns because the simulations do not account for the solid precipitation layer on the liquid interface. Hence, we speculated that, in addition to the non-monotonic surface tension and reaction kinetics, more factors would be involved in the manifestation of the observed oscillatory flows. Upon further inspection of the flow oscillation via image analysis and PIV measurements,

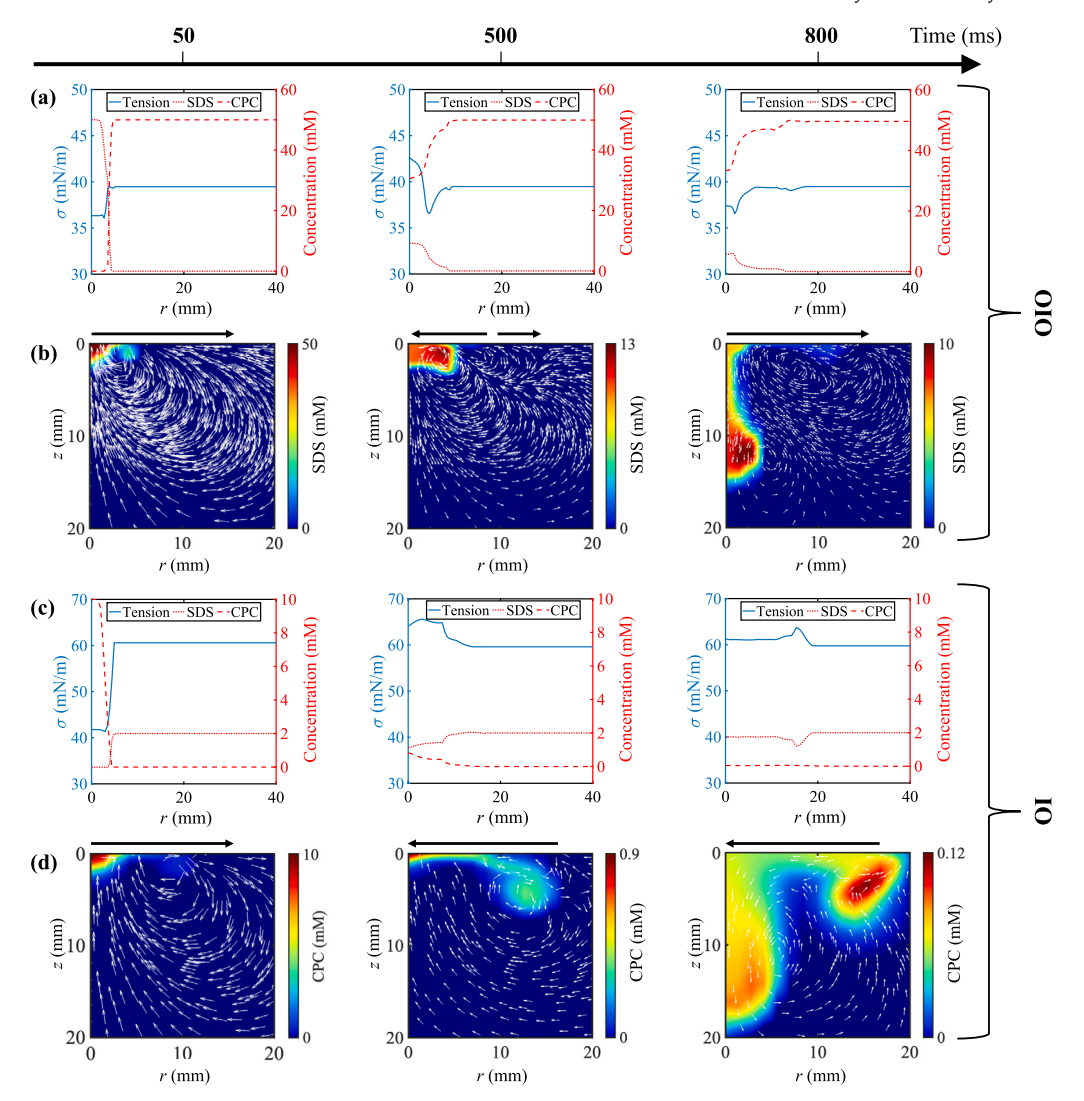


Fig. 5. Numerical simulations of surfactant transport for (a,b) OIO (droplet = SDS, 50 mM; bath = CPC, 50 mM) and (c,d) OI (droplet = CPC, 10 mM; bath = SDS, 2 mM) flows. (a,c) Profiles for the surface tension (solid blue curve), concentration of surfactants from the droplet (dotted red curve), and concentration of surfactants from the bath (dashed red curve) along the air-water interface (z = 0 mm) for (a) OIO and (b) OI flows. (b,d) Droplet surfactant concentration plot for (b) OIO and (d) OI flows. Black arrows represent the direction of fluid flow at the interface. The plots are extracted from Movies S5-S8 (Supporting Materials).

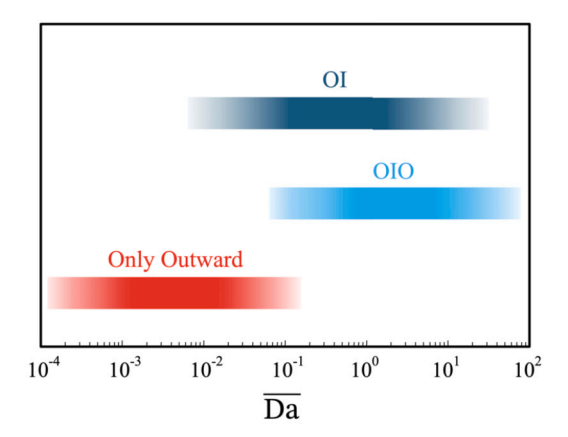


Fig. 6. Spatially averaged Damköhler number obtained from the simulations for various flow patterns.

we hypothesized that this flow is attributed to the interplay between the Marangoni stress and the dissipation of elastic energy from the solid precipitation layer. This finding closely aligns with the recent observations made by Yano et al. involving insoluble surfactants and alcohol molecules [26].

As shown in Fig. 7 (Movie S9), the initial outward Marangoni flow is accompanied by the formation of a solid layer of precipitates resulting from the complexation of oppositely charged surfactants. The precipitation layer darkens over time, indicating a gradual increase in the film thickness. The outward Marangoni flow exhibits an outward stress that is strong enough to cause the precipitation layer to break apart (383 ms, green fragment). This film breakage exposes the unreacted surfactants from the bath to the free surface, which shortly after undergoes reaction with the residual surfactants from the droplet, thus increasing the surface tension and giving rise to reversed Marangoni flow, as shown by red arrows at 416 ms.

The initial outward Marangoni flow has not yet lessened; as soon as the newly created free surface is covered with a new layer of precipitates, the inward flow weakens, enabling the outward flow to prevail once again. Subsequently, the new precipitation layer undergoes disintegration (shown by the yellow fragment at 483 ms in Fig. 7), repeating this cycle until the outward Marangoni flow weakens.

Over time, as the reaction progresses, the fragmented precipitation layer undergoes an expansion in size and thickness, and as a consequence, the surface tension gradient is expected to decrease, which

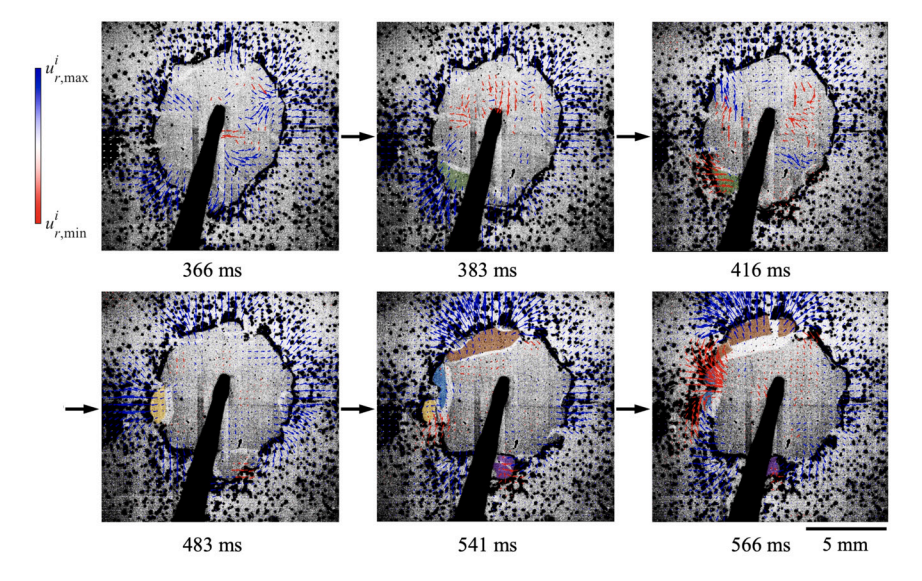


Fig. 7. Image sequence of oscillatory flow resulting from the dynamic interplay between outward and inward Marangoni flows and breakage of solid precipitation film. Droplet = SDS, 25 mM; bath = CPC, 25 mM. Blue arrows indicate radially outward flow ($u_r > 0$) while red arrows indicate inward flow ($u_r < 0$). Each breakage of the precipitation film is false-colored for better visualization. u_r^i represents the maximum and minimum radial velocity at each instance. The video is shown in Movie S9 (Supporting Materials).

should result in a weaker Marangoni flow. Nevertheless, this behavior is not observed through the PIV analysis at later times, as depicted in Fig. 7 (≥ 541 ms), which shows a sudden burst of a strong outward flow. The increased outward flow observed at subsequent times can be explained by the fact that the elastic energy released within the larger fragmented layer upon breakage (shown by the brown fragment at 541 ms) has enough strength to overcome the retraction of the layer through the inward Marangoni stress. The outward movement of the large brown fragment and the inward movement of the small blue fragment are attributed to the size-dependent elastic stress within different precipitation fragments. In the case of the small blue fragment, the inward Marangoni stress is greater than the elastic stress, leading to inward flow, whereas the larger brown fragment experiences elastic stress that is strong enough to surpass the inward Marangoni flow.

3.5. Attractive surfactant interaction drives non-monotonic Marangoni flows

To ensure that the flow reversal and oscillation stem from surfactant interactions, we conduct experiments on different surfactant combinations, utilizing a non-ionic surfactant Triton X-100 (TX) and another cationic surfactant cetyltrimethylammonium bromide (CTAB), in addition to SDS and CPC. Fig. 8 displays the radial flow velocity profiles for the combinations of SDS/CPC and SDS/TX. Unlike the case of a CPC droplet in the SDS bath, which creates an inward Marangoni flow at later times (Fig. 8a), introducing a TX droplet onto a bath of either SDS or CPC did not result in any discernible inward flow, as depicted in Fig. 8b. In addition, a mixture of cationic surfactants, CPC and CTAB, did not induce any noticeable flows in the majority of instances.

Based on these observations, we postulate that the attractive coulombic interactions between cationic and anionic surfactants, which exhibit a significant interaction strength, give rise to the formation of localized concentration gradients that facilitate the complex flow patterns. The interaction strength of surfactant mixtures can be quantified by the interaction parameter β , which is defined as [27]

$$\beta = \frac{1}{(1 - X_1)^2} \ln \left(\frac{Y_1 \text{ CMC}^*}{X_1 \text{ CMC}_1} \right). \tag{3}$$

 X_1 is the mole fraction of surfactant 1 in the surfactant mixture, Y_1 is the mole fraction of surfactant 1 in mixed micelles, CMC_1 is the critical micelle concentration of surfactant 1 in the solution that only consists of

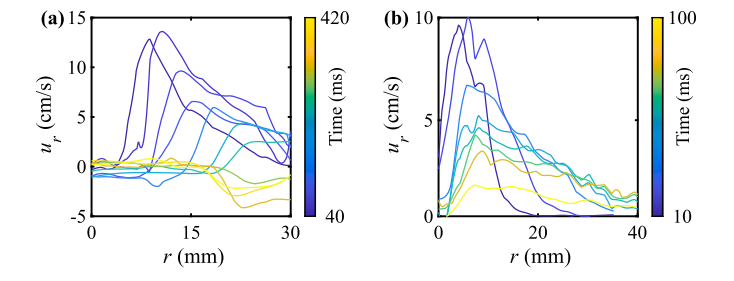


Fig. 8. Impact of surfactant combinations on flow behaviors (a) CPC droplet (10 mM) in SDS bath (1 mM). (b) Triton X-100 droplet (0.25 mM) in SDS bath (1 mM).

surfactant 1, and CMC* is the critical micelle concentration of the mixed surfactant solution. β quantifies the interaction between two dissimilar surfactants relative to the self-interaction of the corresponding pure surfactants before mixing. Negative values indicate attractive interactions, whereas positive values indicate repulsive interactions. When weak interactions occur or no interaction is present, the value falls close to zero [28].

The combination of SDS/CPC is reported to have a relatively large negative value ($-15.9 < \beta < -4.8$) [23], indicating that the attractive interactions are pronounced. On the other hand, TX/CPC mixture exhibits a significantly smaller β value ($\beta=-0.48$) due to a lack of coulombic interactions. Likewise, for CTAB/CPC mixture, the repulsive nature of their coulombic interaction results in mainly small positive β value ($-0.88 < \beta < 2.2$). The correlation between the interaction parameter β and the observed Marangoni flow patterns suggests the underlying cause of complex flow patterns is particularly due to the strong attractive interactions in anionic-cationic surfactant mixtures. This interaction results in distinct flow characteristics that are not observed in other non-attractive surfactant combinations [29–31,12].

3.6. Negligible role of thermal Marangoni effect

Strong coulombic interactions between oppositely charged surfactants can also result in a significant enthalpic change [32–34]. We note that our system may experience thermal Marangoni effect due to the change in the local fluid temperature upon the addition of a droplet to the bath. To ascertain the observed flow behaviors do not stem from

the thermal Marangoni effect, we performed thermal imaging to obtain the temperature change during surfactant complexation. We observed a maximum temperature change of about 1 °C upon introducing droplet to the bath (Fig. S3). With this temperature change, back-of-envelope calculations show that solutal Marangoni flow is dominant, whereas thermal Marangoni flow does not significantly contribute to the flow. For instance, balancing the stresses at the interface gives the solutal and thermal Marangoni velocity as, respectively,

$$u_{S} \approx \frac{\ell_{\perp} \partial_{c} \sigma}{\mu} \nabla_{s} c, \ u_{T} \approx \frac{\ell_{\perp} \partial_{T} \sigma}{\mu} \nabla_{s} T, \tag{4}$$

where μ is the fluid viscosity, ∇_s is the gradient along the interface, and $\partial_{\{c,T\}}\sigma$ is the variation in the surface tension with respect to solute concentration (c) or temperature (T) change [35–37]. ℓ_{\perp} is the momentum diffusion length, which scales as $\ell_{\perp} \sim (\mu \ell_{\parallel}/\rho_f u)^{1/2}$, where ρ_f is the fluid density. Using the numerical simulation and thermal measurement results for the concentration and temperature fields, we find the ratio between the thermal and solutal Marangoni flow as $u_T/u_S = \left(\frac{\partial_T \sigma \nabla_s T}{\partial_c \sigma \nabla_s c}\right)^{2/3} \approx 0.01$. Thus, the solutal Marangoni effect is estimated to be two orders of magnitude stronger than the thermal Marangoni effect, confirming that thermal Marangoni flow is negligible in our system.

4. Conclusion

Prior studies on Marangoni flows have primarily focused on investigating a single type of surfactant and overlooked the examination of irreversible reactions and interactions among multicomponents, particularly at concentrations exceeding CMC, where precipitations and micelles can be formed and alter Marangoni flows [10-14]. In this work, we demonstrated emergent Marangoni flows driven by ionic surfactant interactions. Complex, non-monotonic Marangoni flows found in this work are shown to be sensitive to the concentration and composition of the surfactant mixture, as well as the interaction strength of the surfactant constituents. The surface tension measurements revealed that the mixture of cationic and anionic surfactants has a non-monotonic relationship with the concentration and mixing ratio of surfactants. Such non-linear surface tension is the main reason for the observed nonmonotonic Marangoni flows. Numerical simulations of reactive transport complemented by reaction kinetic measurements provided further insights into the underlying mechanism of each flow pattern. We also demonstrated that the presence of a solid precipitation layer formed by surfactant complexation gives rise to oscillatory flow patterns, where the competing Marangoni stress and elastic stress released within the precipitation layer are expected to drive the oscillatory flows. Further experimental investigations, such as interfacial rheometry, are required to fully elucidate the underlying mechanism of the oscillatory flows.

Additional investigations on other factors that directly impact surfactant reactions, e.g., salinity and temperature, will help to strengthen our understanding of the reaction-driven interfacial flows. Exploring these effects on the multicomponent Marangoni flows is critical, as variations in both the salinity and temperature can have a significant impact on CMC and surfactant precipitation [38,39]. Moreover, incorporating the formation of micelles and precipitates into numerical models, which has been neglected in the current study, will also provide a more robust understanding of the underlying dynamics of the observed oscillating flows.

The findings of the current study have the potential to offer valuable insights into more efficient oil recovery techniques where convective fluxes into confined pores can be induced by interfacial tension gradients to improve the oil extraction [40,41,6]. Additional applications potentially enabled by the radially converging flows (inward flows) reported in this study include the development of effective oil cleanup methods in situations where impaired water reservoirs contain various surfactants. Dispersed oil droplets and slicks may coalesce via the initial outward Marangoni flow, followed by gathering at the center via the

subsequent inward flow to help clean the contaminated surface [11,42]. Ultimately, this understanding may also have implications for controlling the proliferation of waterborne pathogens in contaminated regions, where pathogens are dispersed via Marangoni flows [43,44].

CRediT authorship contribution statement

Ali Nikkhah: Writing – original draft, Visualization, Investigation, Formal analysis, Data curation. **Sangwoo Shin:** Writing – review & editing, Supervision, Resources, Project administration, Funding acquisition, Conceptualization.

Declaration of competing interest

The authors declare that they have no known competing financial interests or personal relationships that could have appeared to influence the work reported in this paper.

Data availability

Data will be made available on request.

Acknowledgements

This material is based upon work supported by the National Science Foundation under Grants No. 2223737 and 2237177.

Appendix A. Supplementary material

Supplementary material related to this article can be found online at https://doi.org/10.1016/j.jcis.2024.07.014.

References

- D.L. Hu, J.W. Bush, The hydrodynamics of water-walking arthropods, J. Fluid Mech. 644 (2010) 5–33.
- [2] D. Kang, M. Chugunova, A. Nadim, A. Waring, F. Walther, Modeling coating flow and surfactant dynamics inside the alveolar compartment, J. Eng. Math. 113 (2018) 23–43.
- [3] A. Nair, G. Sharma, Stability of surfactant-laden liquid film flow over a cylindrical rod, Phys. Rev. E 102 (2) (2020) 023111.
- [4] D. Kang, A. Nadim, M. Chugunova, Marangoni effects on a thin liquid film coating a sphere with axial or radial thermal gradients, Phys. Fluids 29 (7) (2017).
- [5] C. Negin, S. Ali, Q. Xie, Most common surfactants employed in chemical enhanced oil recovery, Petroleum 3 (2) (2017) 197–211.
- [6] S.W. Park, J. Lee, H. Yoon, S. Shin, Microfluidic investigation of salinity-induced oil recovery in porous media during chemical flooding, Energy Fuels 35 (6) (2021) 4885–4892.
- [7] A.Z. Stetten, S.V. Iasella, T.E. Corcoran, S. Garoff, T.M. Przybycien, R.D. Tilton, Surfactant-induced Marangoni transport of lipids and therapeutics within the lung, Curr. Opin. Colloid Interface Sci. 36 (2018) 58–69.
- [8] M. Morciano, M. Fasano, S.V. Boriskina, E. Chiavazzo, P. Asinari, Solar passive distiller with high productivity and Marangoni effect-driven salt rejection, Energy Environ. Sci. 13 (10) (2020) 3646–3655.
- [9] B. Kwak, S. Choi, J. Maeng, J. Bae, Marangoni effect inspired robotic self-propulsion over a water surface using a flow-imbibition-powered microfluidic pump, Sci. Rep. 11 (1) (2021) 17469.
- [10] M.L. Sauleda, H.C. Chu, R.D. Tilton, S. Garoff, Surfactant driven Marangoni spreading in the presence of predeposited insoluble surfactant monolayers, Langmuir 37 (11) (2021) 3309–3320.
- [11] H. Kim, K. Muller, O. Shardt, S. Afkhami, H.A. Stone, Solutal Marangoni flows of miscible liquids drive transport without surface contamination, Nat. Phys. 13 (11) (2017) 1105–1110.
- [12] T.-L. Hsieh, S. Garoff, R.D. Tilton, Marangoni spreading time evolution and synergism in binary surfactant mixtures, J. Colloid Interface Sci. 623 (2022) 685–696.
- [13] A.-D.C. Nguindjel, P.A. Korevaar, Self-sustained Marangoni flows driven by chemical reactions, ChemSystemsChem 3 (6) (2021) e2100021.
- [14] G. Dunér, S. Garoff, T.M. Przybycien, R.D. Tilton, Transient Marangoni transport of colloidal particles at the liquid/liquid interface caused by surfactant convectivediffusion under radial flow, J. Colloid Interface Sci. 462 (2016) 75–87.
- [15] S. Mandre, Axisymmetric spreading of surfactant from a point source, J. Fluid Mech. 832 (2017) 777–792.

- [16] M.L. Sauleda, T.-L. Hsieh, W. Xu, R.D. Tilton, S. Garoff, Surfactant spreading on a deep subphase: coupling of Marangoni flow and capillary waves, J. Colloid Interface Sci. 614 (2022) 511–521.
- [17] B. Sohrabi, H. Gharibi, B. Tajik, S. Javadian, M. Hashemianzadeh, Molecular interactions of cationic and anionic surfactants in mixed monolayers and aggregates, J. Phys. Chem. B 112 (47) (2008) 14869–14876.
- [18] J.D. Berry, M.J. Neeson, R.R. Dagastine, D.Y. Chan, R.F. Tabor, Measurement of surface and interfacial tension using pendant drop tensiometry, J. Colloid Interface Sci. 454 (2015) 226–237.
- [19] Z. Khan, S.A. Al-Thabaiti, E. El-Mossalamy, A.Y. Obaid, Studies on the kinetics of growth of silver nanoparticles in different surfactant solutions, Colloids Surf. B 73 (2) (2009) 284–288.
- [20] D. Kumar, J.M. Khan, M. Posa, A.K. Pulikkal, B. Saha, A. Bhattarai, Effect of quaternary ammonium Gemini surfactant solution on the rate constant of the ninhydrin-lysine reaction, Ind. Eng. Chem. Res. 62 (39) (2023) 15897–15906.
- [21] C.H. Rodriguez, L.H. Lowery, J.F. Scamehorn, J.H. Harwell, Kinetics of precipitation of surfactants. I. Anionic surfactants with calcium and with cationic surfactants, J. Surfactants Deterg. 4 (1) (2001) 1–14.
- [22] S. Chanda, D. Das, J. Das, K. Ismail, Adsorption characteristics of sodium dodecylsulfate and cetylpyridinium chloride at air/water, air/formamide and air/waterformamide interfaces, Colloids Surf. A 399 (2012) 56–61.
- [23] K. Maiti, S. Bhattacharya, S. Moulik, A. Panda, Physicochemistry of the binary interacting mixtures of cetylpyridinium chloride (cpc) and sodium dodecylsulfate (sds) with special reference to the catanionic ion-pair (coacervate) behavior, Colloids Surf. A 355 (1–3) (2010) 88–98.
- [24] N. Watanabe, S. Watase, N. Kadonishi, Y. Okamoto, H. Umakoshi, Revealed properties of various self-assemblies in two catanionic surfactant systems in relation to their polarity and molecular packing state, Langmuir 38 (48) (2022) 14768–14778.
- [25] R. Roskoski, Michaelis-Menten Kinetics, Elsevier, 2015.
- [26] Y.F. Yano, H. Tada, E. Arakawa, W. Voegeli, T. Ina, T. Uruga, T. Matsushita, Periodic elastic motion in a self-assembled monolayer under spontaneous oscillations of surface tension: molecules in a scrum push back a Marangoni flow, J. Phys. Chem. Lett. 11 (15) (2020) 6330–6336.
- [27] A. Bagheri, P. Khalili, Synergism between non-ionic and cationic surfactants in a concentration range of mixed monolayers at an air–water interface, RSC Adv. 7 (29) (2017) 18151–18161.
- [28] B. Kronberg, K. Holmberg, B. Lindman, Surface Chemistry of Surfactants and Polymers. John Wiley & Sons. 2014.
- [29] S. Mukherjee, D. Mitra, S. Bhattacharya, A. Panda, S. Moulik, Physicochemical studies on the micellization behavior of cetylpyridinium chloride and Triton X-100 binary mixtures in aqueous medium, Colloid J. 71 (2009) 677–686.

- [30] H.J. El-Aila, Interaction of nonionic surfactant Triton X-100 with ionic surfactants, J. Dispers. Sci. Technol. 30 (9) (2009) 1277–1280.
- [31] T. Chakraborty, S. Ghosh, S.P. Moulik, Micellization and related behavior of binary and ternary surfactant mixtures in aqueous medium: cetyl pyridinium chloride (CPC), cetyl trimethyl ammonium bromide (CTAB), and polyoxyethylene (10) cetyl ether (Brij-56) derived system, J. Phys. Chem. B 109 (31) (2005) 14813–14823.
- [32] G.J. Papenmeier, J.M. Campagnoli, Microcalorimetry. thermodynamics of the reaction of anionic detergent with a cationic detergent, J. Am. Chem. Soc. 91 (24) (1969) 6579–6584
- [33] K.L. Stellner, J.C. Amante, J.F. Scamehorn, J.H. Harwell, Precipitation phenomena in mixtures of anionic and cationic surfactants in aqueous solutions, J. Colloid Interface Sci. 123 (1) (1988) 186–200.
- [34] P. Norvaisas, V. Petrauskas, D. Matulis, Thermodynamics of cationic and anionic surfactant interaction, J. Phys. Chem. B 116 (7) (2012) 2138–2144.
- [35] M. Roché, Z. Li, I.M. Griffiths, S. Le Roux, I. Cantat, A. Saint-Jalmes, H.A. Stone, Marangoni flow of soluble amphiphiles, Phys. Rev. Lett. 112 (20) (2014) 208302.
- [36] S. Shin, I. Jacobi, H.A. Stone, Bénard-Marangoni instability driven by moisture absorption, Europhys. Lett. 113 (2) (2016) 24002.
- [37] R. Van Gaalen, H. Wijshoff, J. Kuerten, C. Diddens, Competition between thermal and surfactant-induced Marangoni flow in evaporating sessile droplets, J. Colloid Interface Sci. 622 (2022) 892–903.
- [38] F. Goodarzi, S. Zendehboudi, Effects of salt and surfactant on interfacial characteristics of water/oil systems: molecular dynamic simulations and dissipative particle dynamics, Ind. Eng. Chem. Res. 58 (20) (2019) 8817–8834.
- [39] A.F. Belhaj, K.A. Elraies, S.M. Mahmood, N.N. Zulkifli, S. Akbari, O.S. Hussien, The effect of surfactant concentration, salinity, temperature, and ph on surfactant adsorption for chemical enhanced oil recovery: a review, J. Pet. Explor. Prod. Technol. 10 (2020) 125–137.
- [40] M. Masoudi, M. Khosravi, B. Rostami, P. Abolhosseini, Effect of Bénard-Marangoni flow on the bypassed oil recovery: micromodel study, J. Pet. Sci. Eng. 178 (2019) 1067–1078.
- [41] S. Palizdan, J. Abbasi, M. Riazi, M.R. Malayeri, Impact of solutal Marangoni convection on oil recovery during chemical flooding, Pet. Sci. 17 (2020) 1298–1317.
- [42] J. Liu, X. Guo, Y. Xu, X. Wu, Spreading of oil droplets containing surfactants and pesticides on water surface based on the Marangoni effect, Molecules 26 (5) (2021) 1408.
- [43] L. Bourouiba, D.L. Hu, R. Levy, Surface-tension phenomena in organismal biology: an introduction to the symposium, Integr. Comp. Biol. 54 (6) (2014) 955–958, https://doi.org/10.1093/icb/icu113.
- [44] S. Poulain, L. Bourouiba, Disease transmission via drops and bubbles, Phys. Today 72 (5) (2019) 70–71, https://doi.org/10.1063/PT.3.4211.